Energy Reports 8 (2022) 10203–10218

Contents lists available at ScienceDirect

Energy Reports

journal homepage: www.elsevier.com/locate/egyr

Heat transfer analysis of phase change material composited with metal foam-fin hybrid structure in inclination container by numerical simulation and artificial neural network

Wei Cui [a], Tianyu Si [a], Xiangxuan Li [a], Xinyi Li [a], Lin Lu [b], Ting Ma [a], Qiuwang Wang [a,*]

[a] School of Energy and Power Engineering, Xi'an Jiaotong University, Xi'an, 710049, PR China
[b] Department of Building Environment and Energy Engineering, The Hong Kong Polytechnic University, Hong Kong, 999077, PR China

ARTICLE INFO

Article history:
Received 29 January 2022
Received in revised form 16 April 2022
Accepted 31 July 2022
Available online 18 August 2022

Keywords:
Phase change material
Metal foam-fin hybrid structure
Inclination angle
Numerical simulation
Artificial neural network

ABSTRACT

Improving the heat transfer performance of phase change material (PCM) plays a crucial role in designing efficient latent heat thermal energy storage (LHTES) systems. The purpose of this study is to address and elucidate the effects of the metal foam-fin hybrid structure and the inclination angle on the phase change process by using the numerical simulation method. An experimental system for the validation of the numerical models is established. The solid–liquid phase interfaces, streamlines, liquid fraction (f), the dimensionless time ($Fo \times Ste$), and average Nusselt number ($\overline{Nu}$) of PCM in the container enclosure at inclination angles of 0°, 30°, 60°, and 90° with six kinds of enhanced heat transfer structures, including fin, metal foam, and metal foam-fin hybrid structures, are compared. Besides, the liquid fraction and $\overline{Nu}$ during the phase change process are predicted by the artificial neural network (ANN). Results demonstrate that the optimized heat transfer performance of the metal foam-fin hybrid structure could reduce the melting time. In addition, the increase in the number of fins can improve the heat transfer performance and reduce heat accumulation in the top area with the inclination angle increasing. Compared to pure PCM at the inclination angle of 90°, the values of $Fo \times Ste$ of metal foam-1 fin and metal foam-5 fins hybrid structures are reduced by 52.69% and 60.02%, respectively. However, the energy storage density per unit volume decreases as a function of the increasing inclination angles and the number of fins within a case. Furthermore, the excellent predictions of f and $\overline{Nu}$ are obtained by ANN with MSE and R^2 of 9.6480×10^{-5}, 0.9990 and 0.0150, 0.9937, respectively.

1. Introduction

To solve the conflict between energy supply and demand and improve the energy utilization efficiency, latent heat thermal energy storage (LHTES) systems based on phase change material (PCM) offer a broad variety of residential and commercial applications like electronic thermal management (Ling et al., 2014), building energy saving (Tyagi et al., 2021), batteries thermal management (Luo et al., 2022), industrial waste heat management (Li et al., 2019), photovoltaic thermal systems (Alva et al., 2017) and so on. Since PCM can absorb and release heat, it is well-suited for different thermal regulation and thermal energy storage systems due to the attainable advantages of cheap cost, high storage density, and adjustable melting range (Zhang et al., 2018). However, PCM has low thermal conductivity, which lengthens the solid–liquid phase change time, and seriously depresses their practical thermal applications (Ji et al., 2018).

To design efficient LHTES systems, heat transfer enhancement strategies have been developed to improve the heat transfer rate of PCM, such as insertion of fins (Sodhi and Muthukumar, 2021), formation of composite PCM (CPCM) with porous materials (Oya et al., 2012), dispersion of high thermal conductivity nanoparticles (Sami and Etesami, 2017), etc. Among these enhancement strategies, fins are one of the most popular thermal conductivity enhancers due to the ease of fabrication and simplicity in structures, especially in terms of system size. Ali and Arshad (2017) experimentally investigated the efficient thermal management performance based on circular pin-fin heat sinks for passive cooling of electronic devices. The results showed that the pin-fin heat sinks prolonged the working time of the thermal management module and effectively controlled the temperature of electronic devices. Hosseinizadeh et al. (2011) experimentally and numerically investigated the performance of PCM-based heat sink, considering various parameters of number, height, and thickness of fins. The results showed that increasing the number and height of fins led to an appreciable increase in overall thermal

* Corresponding author.
E-mail address: wangqw@mail.xjtu.edu.cn (Q. Wang).

https://doi.org/10.1016/j.egyr.2022.07.178

Nomenclature

A_{mush}	Mushy zone constant
C_i	Inertia coefficient
c_p	Specific heat capacity ($kJ \cdot kg^{-1} \cdot K^{-1}$)
f	Liquid fraction
Fo	Fourier number
H	Height (m)
K	Permeability (m^2)
La	Latent heat ($kJ \cdot kg^{-1}$)
n	Number of fins
Nu	Nusselt number
$\overline{Nu}$	Average Nusselt number
P	Input of DC power supply (W)
q	Heat flux ($W \cdot m^{-2}$)
Q_{loss}	Heat loss
Q_v	Energy storage density per unit volume
Ra	Rayleigh number
S	Source term
Ste	Stefan number
T	Temperature (K)
t	Time (s)
u	Velocity in x direction ($m \cdot s^{-1}$)
v	Velocity in y direction ($m \cdot s^{-1}$)
V	Volume (m^3)

Greek symbols

γ	Thermal expansion coefficient (K^{-1})
δ	Small constant
ε	Porosity
θ	Inclination angle
k	Thermal conductivity ($W \cdot m^{-1} \cdot K^{-1}$)
μ	Dynamic viscosity ($m^2 \cdot s^{-1}$)
ρ	Density ($kg \cdot m^{-3}$)
σ	Experimental uncertainty

Subscripts

0	Initial term
e	Efficient
foam	Metal foam
i	Inertia
m	Melting
mush	Mushy zone
s	Solidification
v	Volume
x, y	Cartesian coordinates (m)

Abbreviations

ANN	Artificial neural network
CPCM	Composite PCM
GA	Genetic algorithm
LHTES	Latent heat storage systems
MLPNN	Multilayer perceptron neural network
MSE	Mean square error
PCM	Phase change material
PPI	Pores per inch
R^2	Correlation coefficient

performance while increasing the thickness of fins resulted in only a little improvement.

Except for the insertion of fins, porous materials are the most promising materials for improving the heat transfer performance of PCM. Among them, the metal foam has been extensively investigated and employed as a typical form of porous material owing to its high open porosity, high specific strength and stiffness, and notably good thermal conductivity for continuous skeleton structures (Xiao et al., 2013). Xiao et al. (2013) composited paraffin with nickel foam and copper foam by vacuum impregnation method. The results indicated that the thermal conductivities of CPCMs with nickel and copper foam were nearly three times and 15 times larger than that of pure paraffin, respectively. Liu et al. (2013) numerically studied the melting characteristics of CPCM filled with copper foam and paraffin in a shell and tube latent heat storage device, and more than seven times better heat transfer performance was found with metal foam than with pure PCM in the LHTES systems.

In contrast, the two previously mentioned strategies, namely fins and foam metal, have significant differences in their intrinsic mechanisms for improving heat transfer performance. The considerably increased thermal contact area is a major reason why the fins enhance the heat transfer performance of the PCM. The heat from sources can be rapidly transferred to the low thermal conductivity PCM through the high thermal conductivity metal fins (Shatikian et al., 2005). The phase change rate of PCM near the fins is significantly improved, but the phase change rate of PCM away from the fins is still at an unsatisfactory level. Unlike the limited ability of fins to enhance thermal conductivity, the continuous skeleton structure of foam metal improves the overall thermal conductivity more significantly, while the foam metal lacks the ability to transfer heat to the deeper PCM interior. To solve this issue, the combination of fins and metal foam is proposed by Guo et al. (2021) for providing better thermal transfer performance as expected. They experimentally investigated the effect of metal foam-fin structure on the thermal energy storage system. The results showed that in comparison with the bare tube, the complete melting time of the fin tube, metal foam tube, and fin-foam hybrid tube could be reduced by 52.81%, 79.61%, and 83.35%, respectively (Guo et al., 2021). Besides, Yang et al. (2020) numerically studied the melting/solidification process of PCM by inserting metal foam into the fin interstitials in a shell-and-tube thermal energy storage unit. The results showed that based on the smooth tube, the complete melting/solidification time with fin-metal foam structure significantly decreased by 85.83% and 95.83%, favoring the potential for further advances in thermal energy storage applications. Zhao et al. (2020) numerically investigated the effect of fins number on the heat transfer rate of PCM and found that under the assumption of constant thickness and volume of fins and PCM, the melting rate firstly increased then decreased with fins number. Yang et al. (2021a) proposed the structure with fins and graded metal foam to further enhance thermal performance and confirmed that the existence of the fins significantly shortened the melting time, and the optimal structure reduced the total melting time by 27.23% and increased the thermal energy storage rate by 36.52%. The main enhancement principle of metal foam-fin structure is that thermal energy from the heat sources is transported through fins deeply into the thermal energy storage unit, and most of thermal energy will be further distributed deeply into PCM through the metallic ligaments of metal foam attached to the fins (Guo et al., 2021). Overall, the foam metal-fin hybrid structure is a promising structure for improving the heat transfer rate of PCM, which has wide application prospect in electronic devices (Ding et al., 2021), thermal energy storage (Yang et al., 2020, 2021b) and so on.

Aside from enhancing the thermal conductivity of PCM, various studies have been conducted to understand the impact of

natural convection on the melting process (Be´nard et al., 1985; Ho and Viskanta, 1984). The intensity of natural convection in liquid PCM relies mostly on the melting time, geometric size of the container (Omari et al., 2011), and inclination arrangement (Ozoe et al., 1975) after a kind of PCM is encapsulated inside the LHTES unit. Kamkari et al. (2014) experimentally studied a rectangular enclosure at different inclination angles and discovered that the enclosure inclination had a significant effect on the development of natural convection flow, heat transfer rate, and melting time of the PCM. Yang et al. (2019) experimentally investigated the melting behaviors of pure PCM and PCM embedded in the metal foam at different inclination angles. The results revealed that the inclination angle had a large impact on the formation and development of natural convection during the melting of pure PCM, but had minimal impact on the PCM embedded in metal foam owing to the domination of heat conduction. It is not difficult to find that the inclination angle of the LHTES unit is closely related to the gravitational field. The heat storage and release efficiency of the LHTES systems may be affected by the inclination angle, which alters gravity acceleration in the vertical direction and hence the strength of natural convection (Kothari et al., 2021). In practical applications, to ensure better thermal management of electronic devices, photovoltaic thermal systems, and so on, the LHTES systems is required to maintain a limited temperature variation at the heating wall (Sathe and Dhoble, 2019; Zheng et al., 2018). Therefore, this places higher demands on the heat transfer rate of PCM at different inclination angles in the LHTES systems.

Additionally, it can be summarized from previous studies on the heat transfer performance of PCM that the nonlinear and dynamic characteristics of the heat transfer process of PCM lead to extremely expensive computational and experimental costs (Xu et al., 2021). Nowadays, more researchers are trying to use the artificial neural network (ANN) to solve complex engineering problems in nonlinear systems with a considerable reduction in computational and experimental costs. Motahar and Jahangiri (2020) predicted the transient heat transfer coefficient of a PCM heat sink using an ANN model. It was found that the proposed ANN predicted the Nusselt number with good accuracy, with a maximum difference of less than 6.0% between experimental data and ANN predictions.

As previously mentioned, the foam metal-fin hybrid structures offer remarkable advantages in terms of improved heat transfer in the LHTES systems. However, it should be noted that the adjustment in attitude of the thermal energy storage unit corresponds to the change of inclination angles of heating wall during the operation in practical application. As far as we know, the heat transfer enhancement mechanism of the metal foam-fin hybrid structure under different inclination angles is still elusive. Therefore, it is worth more in-depth investigations of the effectiveness of the metal foam-fin hybrid structure in the heat transfer performance of PCM, which may provide useful guidelines for practical applications. To this end, the purpose of this paper is to study the heat transfer performance of PCM with a metal foam-fin hybrid structure in an inclination container enclosure by numerical simulation. Paraffin is selected as the PCM, and six kinds of enhanced heat transfer structures are compounded, including fin, metal foam, and metal foam-fin hybrid structures. The inclination angles of the container enclosure are set as 0°, 30°, 60°, and 90°, respectively. ANSYS-FLUENT is employed for numerical simulations of the phase change process of PCM in the six cases. An experimental system for the phase change process of PCM respectively composited with fin and metal foam is established for the validation of the numerical model. The solid–liquid phase interfaces, streamlines, liquid fraction, the dimensionless time ($Fo \times Ste$), and average Nusselt number of PCM under the effects of various heat transfer enhancement structures and inclination angles are compared. To optimize the heat transfer performance of the metal foam-fin hybrid structure, the effect of the number of fins on the energy storage density per unit volume is investigated. Besides, a typical ANN, the multilayer perceptron neural network optimized by the genetic algorithm, is used to predict the liquid fraction and average Nusselt number of PCM during the phase change process.

Table 1
Thermophysical properties of PCM and copper (Cui et al., 2022).

Properties	PCM	Copper
Melting point (K)	301.35	–
Thermal conductivity ($W \cdot m^{-1} \cdot K^{-1}$)	0.35(s), 0.149(l)	380
Density ($kg \cdot m^{-3}$)	850(s), 775(l)	8900
Dynamic viscosity ($m^2 \cdot s^{-1}$)	4.0×10^{-6}	–
Specific heat ($kJ \cdot kg^{-1} \cdot K^{-1}$)	2.89	0.39
Latent heat of fusion ($kJ \cdot kg^{-1}$)	245	–
Thermal expansion coefficient (K^{-1})	1.0×10^{-3}	–

2. Methodology

2.1. Numerical method

The heat transfer process of PCM in the LHTES systems is simulated by the numerical method. Note that the structure of the LHTES systems is simplified appropriately, to keep the constant size of the container enclosure to package PCM in all the simulations.

2.1.1. Physical model

The LHTES systems based on PCM is deliberated as a 2-D container enclosure with dimensions of 40×80 mm^2 on the x-y plane, as shown in Fig. 1(a). The heating side is set at a constant heat flux, while the other sides are adiabatic. To improve the heat transfer performance of PCM, fin and metal foam are used as the heat transfer enhancement structures during the phase change process. Besides, the container enclosure is rotated to four inclination angles ($\theta = 0°$, 30°, 60°, and 90°) in the x-y plane, as drawn in Fig. 1(b).

The schematics of a thermal energy storage system with fin and metal foam are shown in Fig. 2. The thickness and length of the fin are set as 2 mm and 40 mm, respectively. The structural parameters of metal foam are 90% porosity and 10 PPI. The material of the metal foam and fins are assumed to be copper for its good heat transfer capacity. As shown in Fig. 2, six heat transfer enhancement structures in the container enclosures, denoted as Case 1–6, are designed for the LHTES systems: pure PCM, PCM with 1 fin, PCM with metal foam, PCM with metal foam-1 fin, 3 fins, and 5 fins. The numerical study is performed using commercially available PCM with a melting temperature of 301.35 K. The thermophysical properties of PCM and copper are presented in Table 1.

2.1.2. Mathematical model

The phase change process in the PCM-based LHTES systems is simulated by the enthalpy-porosity method proposed by Voller and Prakash (1987). To simplify the mathematic model, the following assumptions are made during the numerical analysis:
(1) Copper foam is homogeneous and isotropic;
(2) The liquid PCM is incompressible and subjected to the Boussinesq approximation, and its flow in the pore is laminar;
(3) The parameters of the thermal performance of PCM during the phase change process can be considered as constants;
(4) The volume change of molten PCM and the motion of solid PCM are disregarded during the phase change process.

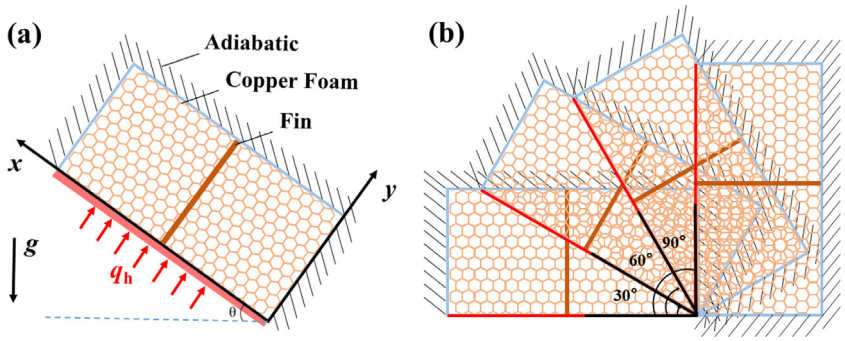

Fig. 1. (a) Numerical configuration and boundary condition, and (b) four inclination angles of 0°, 30°, 60°, and 90°.

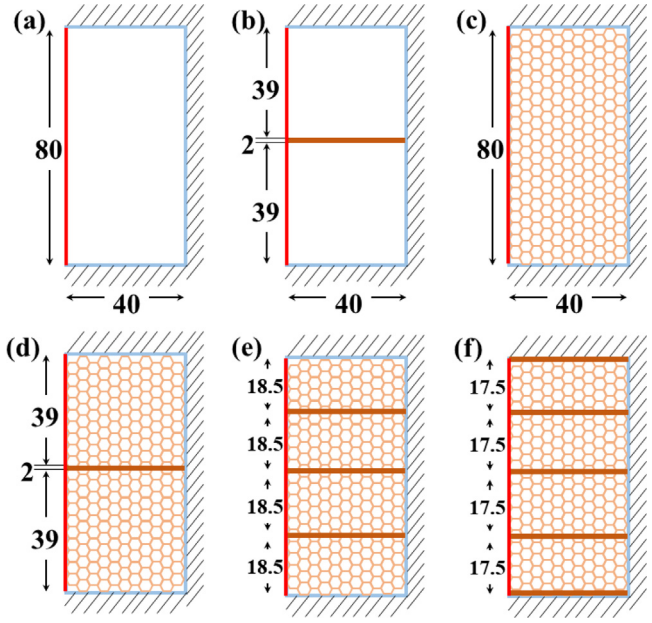

Fig. 2. Physical model of different layouts of fins and metal foam. (a) Case 1: Pure PCM, (b) Case 2: PCM with 1 fin, (c) Case 3: PCM with metal foam, and (d–f) Cases 4–6: PCM with metal foam-1, 3 and 5 fin(s).

According to the preceding assumptions, the continuity, momentum, and energy equations are described as follows (Zheng et al., 2018; Tian and Zhao, 2011):

Continuity equation:

$$\frac{\partial u}{\partial x}+\frac{\partial v}{\partial y}=0 \tag{1}$$

Momentum equations:

$$\frac{\rho}{\varepsilon}\left(\frac{\partial u}{\partial t}+\frac{1}{\varepsilon}\left(u\frac{\partial u}{\partial x}+v\frac{\partial u}{\partial y}\right)\right)=\frac{\mu}{\varepsilon}\left(\frac{\partial^2 u}{\partial x^2}+\frac{\partial^2 u}{\partial y^2}\right)-\frac{\partial P}{\partial x}+S_x \tag{2}$$

$$\frac{\rho}{\varepsilon}\left(\frac{\partial v}{\partial t}+\frac{1}{\varepsilon}\left(u\frac{\partial v}{\partial x}+v\frac{\partial v}{\partial y}\right)\right)=\frac{\mu}{\varepsilon}\left(\frac{\partial^2 v}{\partial x^2}+\frac{\partial^2 v}{\partial y^2}\right)-\frac{\partial P}{\partial y}+S_y \tag{3}$$

where S_x and S_y in Eqs. (2) and (3) are written as :

$$S_x=A_{\text{mush}}\frac{(1-\beta)^2}{\beta^3+\delta}u-\frac{\mu}{K}u-\frac{\rho C_i}{\sqrt{K}}|u|\,u+\rho g\gamma\,(T-T_0)\sin\theta \tag{4}$$

$$S_y=A_{\text{mush}}\frac{(1-\beta)^2}{\beta^3+\delta}v-\frac{\mu}{K}v-\frac{\rho C_i}{\sqrt{K}}|v|\,v+\rho g\gamma\,(T-T_0)\cos\theta \tag{5}$$

where the impact of the mushy region during the phase change process is described by the first term on the right side of Eqs. (4) and (5). A_{mush} and δ in this term are set as 10^5 and 10^{-3}, respectively. On the right side of Eqs. (4) and (5), the second and third terms based on the Darcy–Forchheimer law are used to describe liquid flow in porous materials, where K is the permeability and C_i is the inertia coefficient, and the values of two parameters are calculated using the model described in Fourie and Du Plessis (2002). And the final term on the right side of Eqs. (4) and (5) reflect the Boussinesq approximation, which accounts for density fluctuations caused by buoyancy forces and natural convection caused by temperature differences within the liquid PCM.

Energy equation:

$$\left[(1-\varepsilon)\left(\rho c_p\right)_{\text{foam}}+\varepsilon\left(\rho c_p\right)_{\text{PCM}}\right]\frac{\partial T}{\partial t}+\left(\rho c_p\right)_{\text{PCM}}\left(u\frac{\partial T}{\partial x}+v\frac{\partial T}{\partial y}\right)=k_e\left(\frac{\partial^2 T}{\partial x^2}+\frac{\partial^2 T}{\partial y^2}\right)-\varepsilon\rho L\frac{\partial f}{\partial t} \tag{6}$$

f denotes the liquid fraction, which characterizes the phase change process as a function of temperature and is determined by Eq. (7) as follows:

$$f=\begin{cases}0 & T<T_m\\ \dfrac{T-T_s}{T_m-T_s} & T_s<T<T_m\\ 1 & T>T_s\end{cases} \tag{7}$$

For the convenience of analysis, the non-dimensional parameters, including Fourier number (Fo), Stefan number (Ste), and average Nusselt number ($\overline{Nu}$), are defined to describe the phase change process of CPCM in this study, which can be obtained from Eq. (8) as follows:

$$\begin{cases}Fo=\dfrac{kt}{\rho C_p H^2}\\ Ste=\dfrac{C_p qH}{kLa}\\ \overline{Nu}=\dfrac{qH}{k(\overline{T_w}-T_m)}\end{cases} \tag{8}$$

where k, ρ, C_p, La, and T_m represent the thermal conductivity, density, specific heat capacity, latent heat, and melting temperature of PCM, respectively. t and q are the heating time and heat flux. $\overline{T_w}$ is the average temperature of the heating wall. H is the characteristic length of the container enclosure. Note that in the present study, the value of Ste is kept constant.

2.1.3. Initial and boundary conditions

The initial condition and boundary condition are described as follows:

Initial condition:

$$0\le x\le 40,\ 0\le y\le 80,\ u=v=0,\ T_0=297 \tag{9}$$

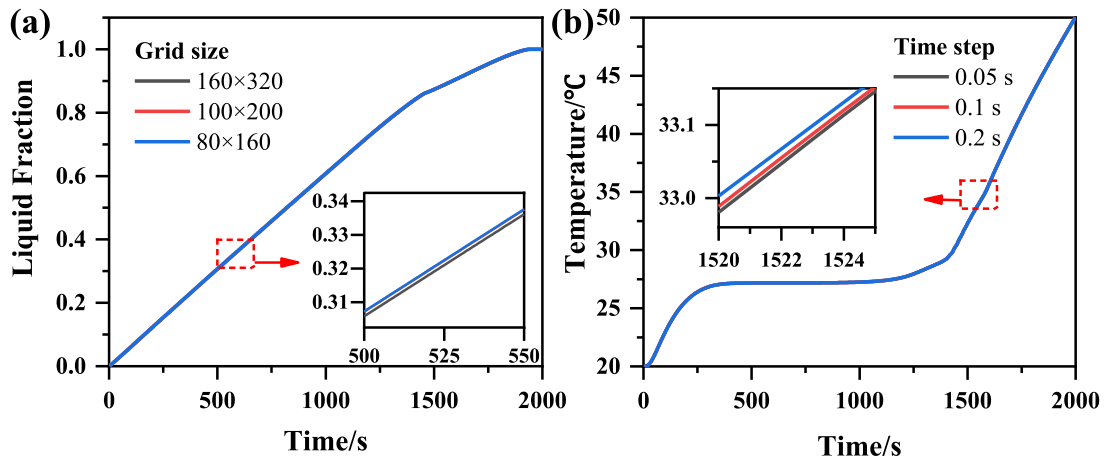

Fig. 3. (a) Grid size independence analysis. (b) Time step independence analysis.

Boundary conditions:

$$x = 0, 0 \le y \le 80, q = 4500 \quad (10)$$

$$x = 40, 0 \le y \le 80, q = 0 \quad (11)$$

$$0 \le x \le 40, y = 0, q = 0 \quad (12)$$

$$0 \le x \le 40, y = 80, q = 0 \quad (13)$$

2.1.4. Numerical procedure

In the numerical simulation, the uniformly structured mesh with quadrilateral cells is used to investigate the phase change process of PCM. The Solidification/Melting model with double precision is used for the numerical calculation by using ANSYS-FLUENT software. The governing equations of mass, momentum, and energy are discretized by the finite volume method in an unsteady solver. Pressure–velocity coupling is accomplished using the SIMPLE method. To discretize the pressure and momentum, we use the PRESTO method and the second order upwind scheme. The convergence criterion for the residuals for continuity equation, velocity, and energy equation is set as 10^{-4}, 10^{-4}, and 10^{-6}, respectively (Zheng et al., 2018).

Different grid sizes and time steps are selected and tested to ensure the independence of the two parameters from the simulation results, based on a comparison of the liquid fraction. Fig. 3(a) shows the difference in the liquid fraction in cases of 80 × 160, 100 × 200, and 160 × 320 grid sizes. Based on the comparison, it can be found that the liquid fraction evolution curves with the three grid sizes display negligible deviations, and the relative error of the liquid fraction is less than 0.43% as the grid size decreases from 100 × 200 to 160 × 320, suggesting that the grid size of 100 × 200 is adequate for the subsequent numerical simulations. Considering the effect of the time step on the accuracy and computational costs of numerical simulations, the time steps of 0.05 s, 0.1 s, and 0.2 s are considered for comparisons of the temperature, as shown in Fig. 3(b). The relative errors are within 0.5% for the above time steps, and the maximum deviation between the liquid fraction for the time step of 0.05 s and 0.1 s is within 0.12%. Therefore, the time step of 0.1 s is selected for the present numerical simulations.

2.1.5. Validation of numerical model

To validate the numerical model, an experimental system for the phase change process of PCM is established, and the schematic diagram and real apparatus are displayed in Figs. 4(a) and (b). The system consists of three parts: test section, electrical heating section, and data acquisition section. A 40 × 80 × 80 mm^3 acrylic container with the two enhanced heat transfer structures of fins and metal foam is filled with PCM by the vacuum impregnation method to reduce the thermal resistance of the phase change process, and the whole is regarded as the thermal energy storage cell. The inclination angles of the test section are adjusted by the bracket. A polyimide electrical heating film with dimensions of 80 × 80 mm^2 is attached to the heating wall fabricated by a copper plate, providing constant and uniform heat flux for the PCM. The heat flux is accurately determined by recording the electric voltage and current of the DC power supply. T-type thermocouples are separately arranged in the thermal energy storage cell with fins and metal foam to monitor the transient temperature. To further minimize the heat loss to the surroundings, all surfaces of the test section are covered by styrofoam insulation material for the thermal insulation from the ambient environment.

In this experiment, the uncertainty is mainly attributed to inaccuracies in the input of DC power supply, thermocouples, and heat loss. Fluctuations in voltage and current affect the input of the DC power supply with a maximum deviation of 3.2%. The accuracy of T-type thermocouples is ±0.3 °C, resulting in the uncertainty of 0.4%. The heat loss of the thermal energy storage cell is estimated with an uncertainty of 4.2%. The uncertainty of the experiment is 5.3%, which can be calculated as the following Eq. (14):

$$\sigma = \sqrt{\left(\frac{\Delta P}{P}\right)^2 + \left(\frac{\Delta T}{T}\right)^2 + \left(\frac{Q_{loss}}{Q}\right)^2} \times 100\% \quad (14)$$

where σ is the uncertainty of the experiment, and P, T, and Q denote the input of DC power supply, temperature, and thermal energy, respectively.

Furthermore, aiming to verify the heat transfer performance enhanced by the metal foam-fins hybrid structure, the present study compares the experimental results of Guo et al. (2021). A concentric cylindrical thermal energy storage tube with a length of 270 mm, an inner diameter of 90 mm, and an outer diameter of 100 mm is accomplished, which is filled with Paraffin 52–54 as PCM. The annular copper foam with the pore density of 10 PPI and the porosity of 0.97 is adopted. The initial temperature of PCM is set at 20.2 °C. The whole experimental cell is heated by the heat transfer fluid with the flow rate of 0.2 m/s and 70 °C, and the other surfaces are considered adiabatic.

The experimental and numerical temperatures of PCM with fins, metal foam, and metal foam-fins hybrid structure are compared in Figs. 5(a), (b) and (c). An acceptable agreement can be

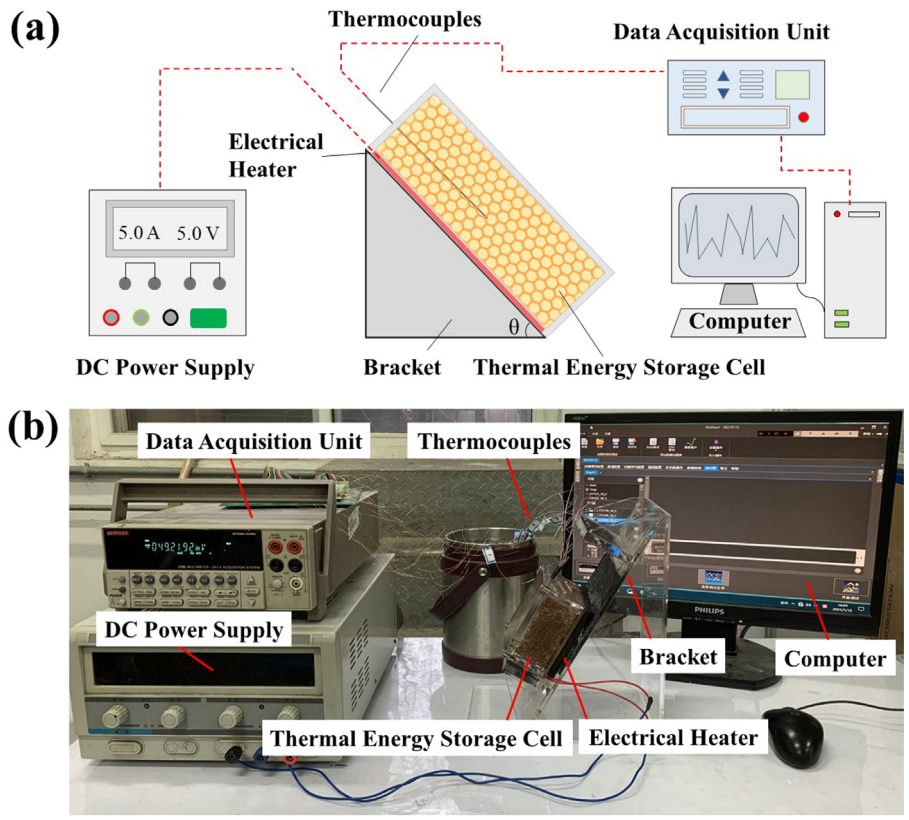

Fig. 4. (a) Schematic diagram and (b) real apparatus of the experimental system for the phase change process of PCM.

obtained between the two methods, and the maximum deviation of temperature between them is less than 5%. The temperature trends of the measurement points in the experiment and numerical simulation are mostly similar, encompassing the three stages before, during, and after the phase change. An accurate numerical model has been constructed by the above quantitative and qualitative comparisons between experiment and numerical simulation, which is then used to support further discussions.

2.2. Artificial neural network

Artificial neural network (ANN) is generally regarded as a computational technique in artificial intelligence systems that offers an alternate method of simulating difficult and ill-defined issues. Among ANN methodologies, the feed-forward multilayer perceptron neural network (MLPNN) is likely to be the most popular topology for function approximation and regression-based studies. In this study, an innovative MLPNN is proposed to predict the phase change process of PCM at four inclination angles based on the results of numerical simulations.

As shown in Fig. 6, the structure of MLPNN consists of an input layer, hidden layer, and output layer. Considering the effects of melting time ($Fo{\times}Ste$), inclination angles (θ), and number of fins (n) on the phase change process of PCM, the inputs of the MLPNN are presented as $X = \{Fo{\times}Ste,\ \theta,\ n\}$, which are independent variables. Besides, the parameters of liquid fraction (f) and $\overline{Nu}$ can be used as dependent variables to describe the phase change process of CPCM, which are presented as the outputs of the MLPNN of $Y = \{f, \overline{Nu}\}$. In general, MLPNN has an arbitrary number of layers, and each layer can be arranged with any number of neurons. To reduce the difference between the actual and predicted values, the MLPNN is trained to change the weights and biases of neurons. Finally, the weighted inputs are added by the neurons, and the results are then subjected to a linear or nonlinear function to determine the output.

Indeed, an appropriate training algorithm and the number of neurons are important to designing the MLPNN. To train and test the MLPNN, the numerical datasets from Cases 3, 4, 5, and 6 are randomly divided into two parts, including 75% as training datasets and 25% as testing datasets. Genetic algorithm (GA) is used to optimize the structure of MLPNN, where the neural network using GA is denoted as the MLP-GA model. To begin with, the MLP-GA model generates a random population depending on the input ranges. It evaluates the fitness functions obtained with the initial population and ranks the solutions based on nondominated sorting. Through the selection, crossover, and mutation operations on individuals in the population, the GA determines the survival of the fittest, to meet the requirements of inheriting the information of the previous generation and being superior to the previous generation. Finally, the procedure is repeated until the termination condition is satisfied. The flow chart of the MLP-GA model is presented in Fig. 7. In this study, 100 units of the population are presumed with crossover and mutation probability as 0.2 and 0.1, respectively.

The number of generations is 100. Besides, the tansig and pureline functions are considered the transfer functions for the hidden and output layer in the structure of MLPNN, as shown in Eqs. (15) and (16).

$$tansig(x) = \frac{e^{x} - e^{-x}}{e^{x} + e^{-x}} \tag{15}$$

$$purelin(x) = x \tag{16}$$

To determine the number of neurons in the structure of MLPNN, a systematic trial-and-error procedure is employed in this study. The statistical accuracy criteria are used to evaluate the predictive performance, including mean square error

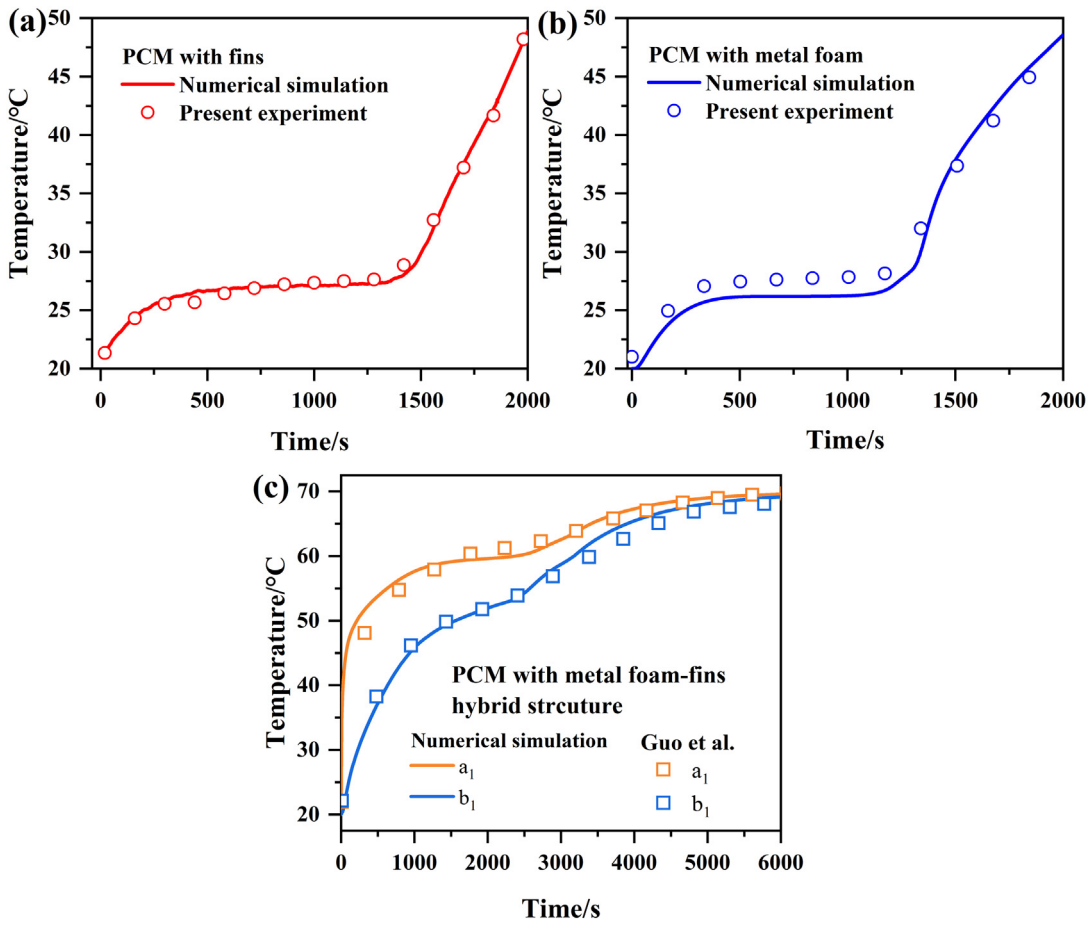

Fig. 5. Comparisons of temperature between numerical simulation and the present experiment and Guo et al. (2021), (a) fins, (b) metal foam, and (c) metal foam-fins hybrid structure.

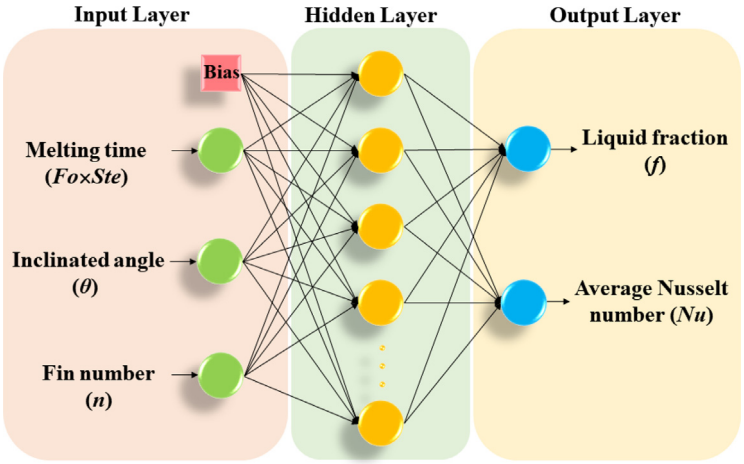

Fig. 6. Structure of MLPNN for predicting the phase change process of CPCM.

(MSE) and correlation coefficient (R^2), which are obtained by the following Eqs. (17)–(18).

$$MSE = \frac{1}{n}\sum_{i=1}^{n}(Y_i^{exp} - Y_i^{pred})^2 \tag{17}$$

$$R^2 = 1 - \frac{\sum_{i=1}^{n}(Y_i^{exp} - Y_i^{pred})^2}{\sum_{i=1}^{n}(Y_i^{exp} - \overline{Y}_i^{exp})^2} \tag{18}$$

3. Results and discussion

3.1. Effects of metal foam-fin hybrid structure with various inclination angles on heat transfer performance

To understand the role of metal foam-fin hybrid structure with various inclination angles in improving heat transfer performance for LHTES systems, the phase change processes for PCM of Cases 1, 2, 3, and 4 are compared.

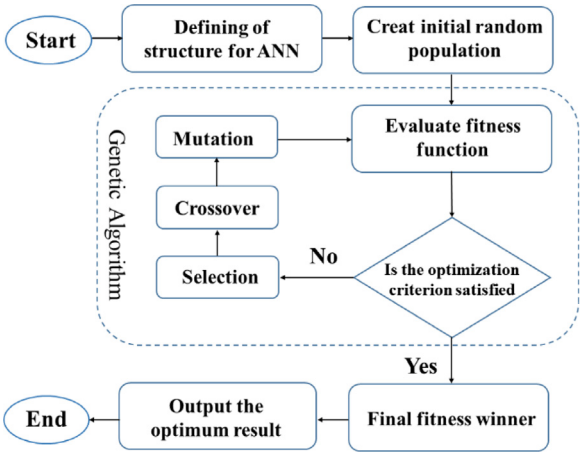

Fig. 7. Computational flow chart of MLP-GA model.

Fig. 8 demonstrates the comparisons of solid–liquid phase interfaces and streamlines of Cases 1 to 4 at four inclination angles during the phase change processes. The values of the dimensionless time ($Fo \times Ste$) in Figs. 8(a)–(d) and (e)–(h) are 0.081 and 0.324, respectively. At the $Fo \times Ste$ of 0.081, four cases show a representative structure of the fluid dynamic characterized by multi-cellular flow patterns, which are called the Rayleigh–Bénard cells (Parsazadeh et al., 2021). For Cases 1 and 2, due to the influence of Rayleigh -Bénard convection, the solid–liquid interfaces of pure PCM are uneven. With the increase of the inclination angle, driven by the buoyance force, molten PCM with higher temperature rises to the top of the container along the heating wall, and molten PCM with lower temperature moves to the bottom of the container enclosure along with the solid PCM, which results in a higher melting rate of PCM in the upper region than in the lower region of the container enclosure. Hence, the solid–liquid phase interfaces of PCM for Cases 1 and 2 become slightly inclined and show a more obvious trend with the increase of inclination angle, as shown in Figs. 8(a) and (b). However, for Cases 3 and 4, the solid–liquid phase interfaces of CPCM almost keep parallel to the heating wall, with the inclination angle increasing from 0° to 90° at the initial stage, as shown in Figs. 8(c) and (d). This indicates that the heat transfer from the heating wall to the solid PCM is dominated by heat conduction at the initial stage of the phase change process. It is also noted from the streamlines that the Rayleigh–Bénard cells exist in the liquid layer for Cases 3 and 4.

With the heating time prolonged, the thickness of liquid PCM increases, and convection heat transfer takes overheat conduction. At the $Fo \times Ste$ of 0.324 and the inclination angle of 0°, the solid–liquid phase interfaces of four cases are parallel to the heating wall. But as the inclination angle increases to 30°, 60°, and 90°, the melting rate at the bottom is significantly lower than that at the top, and the four cases display the inclined solid–liquid phase interfaces, as shown in Figs. 8(e)–(h).

Additionally, it is mentioned that PCM near the fin melts faster showing the high heat transfer performance. This demonstrates that with the inclusion of fin for improving the heat transfer, heat from the heating wall can be carried into the interior of PCM by the fin and then absorbed by PCM.

To get a deep understanding of the effects of metal foam-fin hybrid structure with various inclination angles on the heat transfer performance, the liquid fraction for the four cases is plotted in Fig. 9. From a global perspective, it can be observed that the melting rate for Case 4 is the highest among the four structures, followed by Case 3, 2, and 1. At the initial stage, the liquid fraction curves of Cases 2, 3, and 4 almost overlap, except for Case 1, due to the contribution of additional fin or metal foam to heat transfer. As the melting progresses, the liquid fraction of Case 3 and 4 is higher than that for Case 2, indicating that the improvement of heat transfer performance for the PCM embedded with metal foam is higher than that for the PCM inserted with the fin. For the comparison of the liquid fraction of Case 3 and 4, it can be inferred that the metal foam-fin hybrid structure in Case 4 can improve the heat transfer capability, resulting in a higher liquid fraction than that for Case 3. Besides, it is worth noting that the melting rate of four cases decreases as the inclination angle increases from 0° to 90°, as shown in Fig. 9. Based on the previous analysis, the effect of thermal buoyancy forces on convective heat transfer becomes more significant as the inclination angle increases.

Table 2
Values of $Fo \times Ste$ for four cases at four inclination angles.

Case	$Fo \times Ste$			
	0°	30°	60°	90°
1	0.567	0.620	0.841	1.108
2	0.502	0.610	0.751	0.961
3	0.485	0.510	0.525	0.542
4	0.461	0.506	0.509	0.524

To quantitatively analyze the heat transfer capability, the values of $Fo \times Ste$ for the full melting ($f = 1.0$) for four cases are summarized in Table 2. Taking the inclination angle of 90° for example and setting Case 1 as the comparison basis, the values of $Fo \times Ste$ are reduced by 13.29%, 51.06%, and 52.69% for Cases 2, 3, and 4, respectively. Case 4 at an inclination angle of 0° presents the optimized heat transfer performance and Case 1 at an inclination angle of 90° shows the undesirable heat transfer performance. It is demonstrated that the simultaneous participation of fins and metal foam, as well as the flat placement of the LHTES device, can shorten the total melting time, which can aid in the practical application of LHTES technology.

The value of $\overline{Nu}$ represents the intensity of the convection heat transfer during the phase change process of PCM, related to the average temperature of the heating wall, based on the definition of $\overline{Nu}$ in Eq. (8). Aiming to further discuss the heat transfer process of the PCM, Fig. 10 depicts the $\overline{Nu}$ for Cases 1, 2, 3, and 4 at four inclination angles varying with $Fo \times Ste$. Globally speaking, the $\overline{Nu}$ for Case 4 is higher than that for the other three cases at four inclination angles in the phase change process, as shown in Fig. 10, indicating that the average temperature of the heating wall for Case 4 is relatively lower, attributed to the remarkable heat transfer performance of the metal foam-fin hybrid structure. Besides, it can be found that in the initial stage of the phase change process, the slight difference in $\overline{Nu}$ is observed between Cases 3 and 4. This phenomenon is explained by the fact that in the initial stage the heat transfer is dominated by conduction, and the addition of fins to the foam metal has an extremely weak effect on improving heat transfer performance in this stage. However, the $\overline{Nu}$ for Case 4 drops slower than that of Case 3 with the heating time prolonged, which is caused by the insertion of fins that affect the intensity of the convection heat transfer. In addition, it can be found that the $\overline{Nu}$ of Cases 1 and 2 almost overlaps at four inclination angles, demonstrating the limited improvement in heat transfer performance of PCM with the addition of fins alone.

Overall, the metal foam-fin hybrid structure provides the optimal heat transfer performance of PCM compared with the fin and the metal foam. The heat transferred via the fins is successfully absorbed by the PCM around the fins during the heat storage process. Through its rich specific surface area and highly-conducting skeletons, metal foam efficiently transfers heat to

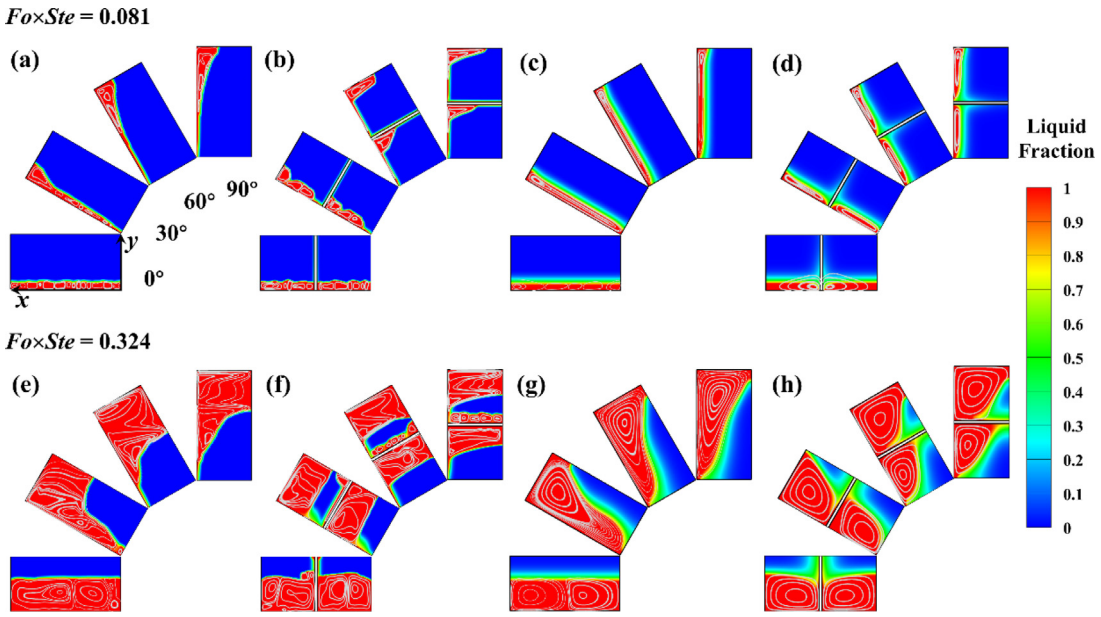

Fig. 8. Transient solid–liquid phase interfaces and streamlines at four inclination angles during the phase change processes, (a) and (e) Case 1, (b) and (f) Case 2, (c) and (g) Case 3, and (d) and (h) Case 4.

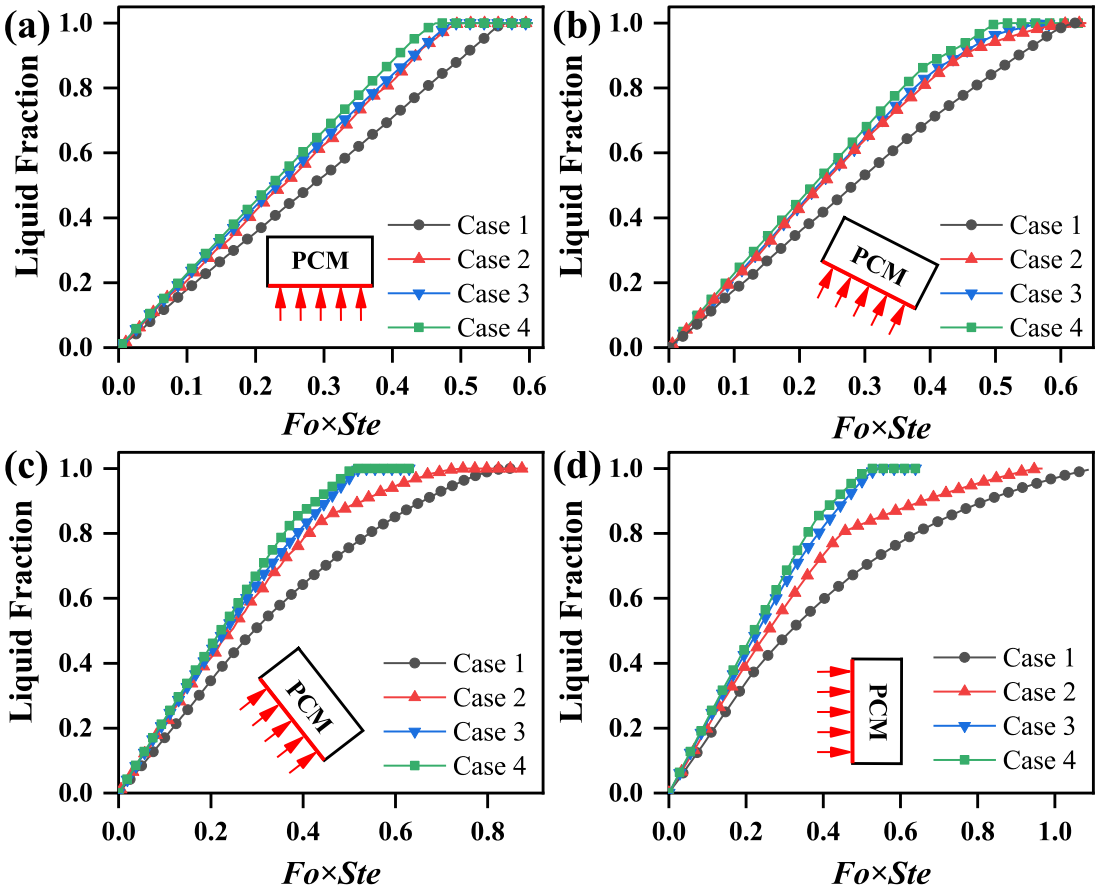

Fig. 9. Comparison of liquid fraction for Cases 1, 2, 3, and 4 at inclination angles of (a) 0°, (b) 30°, (c) 60°, and (d) 90°.

the internal PCM. In practical applications such as photovoltaic thermal systems, if it is necessary to quickly obtain photovoltaic thermal energy from the heat source like the photovoltaic flat-plate collector, it is recommended to insert fins and metal foam

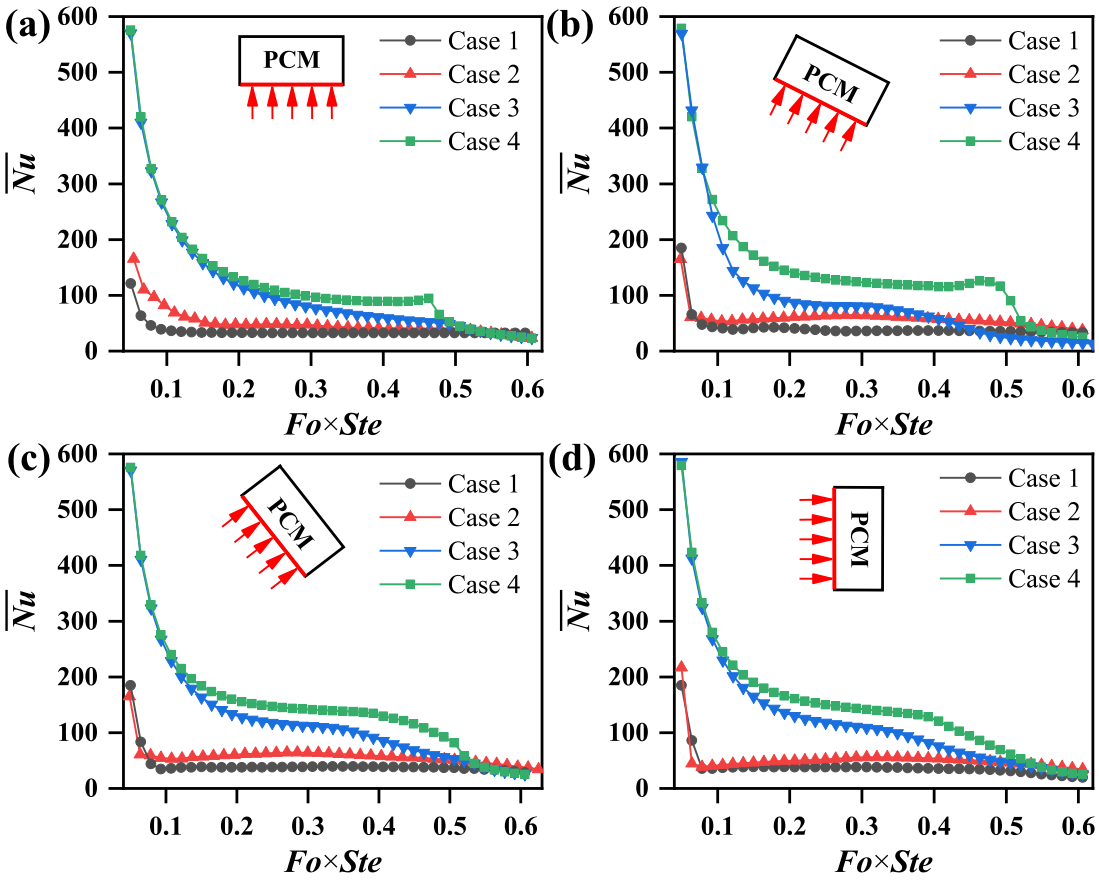

Fig. 10. Comparison of average Nusselt number for Cases 1, 2, 3, and 4 at inclination angles of (a) 0°, (b) 30°, (c) 60°, and (d) 90°.

into the PCM and decrease the inclination angle of the LHTES systems for the goal of reducing heat accumulation in time and improving energy utilization efficiency.

3.2. Effect of number of fins on the heat transfer performance

As previously mentioned, the PCM near fins is melted earlier and faster than that in other regions. Hence, it is essential to clarify the effects of the number of fins in the metal foam-fin hybrid structure on heat transfer performance. To address this issue, the comparisons on the metal foam-1, 3, and 5 fin(s) hybrid structure at four inclination angles of 0°, 30°, 60°, and 90° are carried out towards minimizing melting time.

Fig. 11 illustrates the comparisons of transient solid–liquid phase interfaces and streamlines for Cases 4, 5, and 6 at four inclination angles and $Fo \times Ste$ of 0.081 and 0.324 during the phase change processes. With the inclination angle increasing from 0° to 90°, Cases 4, 5, and 6 present the solid–liquid phase interfaces of CPCM parallel to the heating wall at the $Fo \times Ste$ of 0.081, as shown in Figs. 11(a), (b), and (c). This is mostly owing to the excellent heat conductivity of metal foam and the partitioning of the melting region by the fins. It can be observed from the streamlines of Cases 4, 5, and 6 that the metal foam facilitates a more uniform flow field (Guo et al., 2021). Besides, the fins not only transfer heat from the heating wall but also reduce the height of the liquid PCM flow to form smaller vortices, thus improving heat transfer performance (Sodhi and Muthukumar, 2021). Especially at an inclination angle of 0°, the number of vortices formed increases as the number of fins increases, as shown in Figs. 11(a), (b), and (c).

At the $Fo \times Ste$ of 0.324, significant differences can be found at the solid–liquid phase interfaces for Cases 4, 5, and 6. With the number of fins increasing, the melting rate of Case 6 is notably faster than that of the other two cases at the corresponding inclination angles. This confirms that adding more fins improves the heat transfer performance during the phase change process. An interesting phenomenon is that at an inclination angle of 0°, the solid–liquid phase interface is no longer parallel to the heating wall and grows upward, and a distinct bump appears in the partitioned region as shown in Figs. 11(d), (e), and (f). This special solid–liquid phase interface is formed by the insertion of more fins providing more heating surface for the phase change process of CPCM, leading to a preferential melting of CPCM near the fins. Furthermore, at the same inclination angles of 30°, 60°, and 90°, the solid–liquid phase interface in the partitioned region divided by the fins also differs significantly within a case. As evidenced in Figs. 11(d), (e), and (f) that the melting rate in the partitioned area near the top is distinctly higher than that in the partitioned area at the bottom, which is mainly caused by the convection heat transfer of the liquid PCM in the partitioned area. The top partitioned area is able to benefit from the upward heat transfer in the immediate lower partitioned area through the fins so that the average temperature of the top partitioned area is always higher than that of the lower partitioned area (Sodhi and Muthukumar, 2021). Based on the above results, it is undeniable that the introduction of fins further makes full use of the high thermal conductivity of metal foam to improve the heat transfer performance, while also causing discontinuous flow of the liquid PCM and significant temperature gradients in the inclination container enclosure.

Fig. 12 shows the quantitative comparison of liquid fractions for three cases at four inclination angles during the phase change processes. The melting rate for Case 6 is the highest among the three structures, followed by Cases 5 and 4. When the liquid

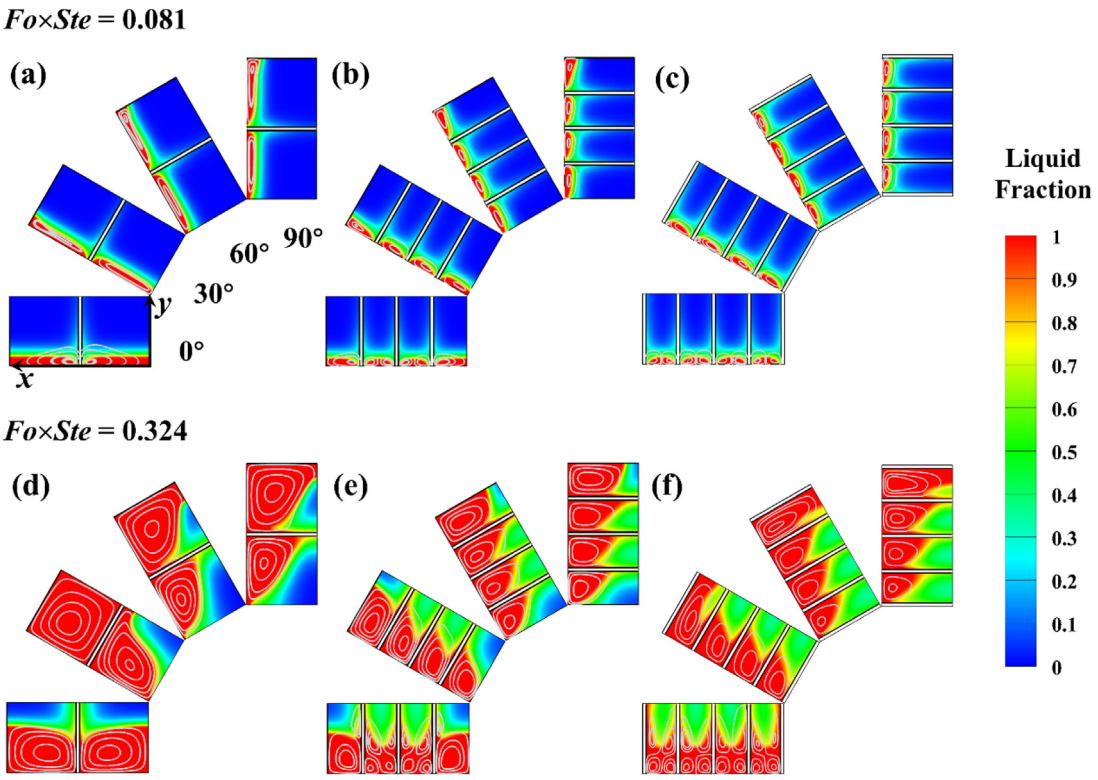

Fig. 11. Transient solid–liquid phase interfaces and streamlines at four inclination angles during the phase change processes, (a) and (d) Case 4, (b) and (e) Case 5, and (c) and (f) Case 6.

fractions are below 0.2 at four inclination angles, the curves of the liquid fraction for the three cases follow the same trend. When the liquid fractions exceed 0.2 at four inclination angles, Case 6 with more fins shows a satisfactory melting rate. It indicates that in the initial stage, compared to the effective role of metal foam with high thermal conductivity performance, the effect of increasing the number of fins on improving the melting rate of CPCM is weak. However, as the phase change process proceeds, the heat transfer performance of the fins is fully utilized in synergy with the rapid thermal conductivity of the metal foam, and the metal foam-fin hybrid structure shows a faster melting rate of CPCM with the number of fins increasing. Furthermore, Fig. 12 illustrates the melting rate of CPCM for three cases decreases as the inclination angle increases from 0° to 90°. Similarly, the change in thermal buoyancy forces due to the increase in tilt angle causes a difference in the performance of convective heat transfer in the phase change process.

Table 3 lists the values of $Fo \times Ste$ for the full melting for three cases at four inclination angles. Still taking the inclination angle of 90° for example and setting Case 1 as the comparison basis, the values of $Fo \times Ste$ are reduced by 52.69%, 56.50%, and 60.02% for Cases 4, 5, and 6, respectively. Case 6 at an inclination angle of 0° presents the optimal heat transfer performance. It is proved that increasing the number of fins as well as flat positioning of LHTES devices may offer optimal heat transfer improvement and minimize the whole melting time, hence assisting in the practical implementation of LHTES technology.

To evaluate the effects of the number of fins on the heat transfer performance, the $\overline{Nu}$ for Cases 4, 5, and 6 at four inclination angles varying with $Fo \times Ste$ are illustrated in Fig. 13. Overall, compared to Cases 4 and 5, Case 6 has a higher $\overline{Nu}$ at four inclination angles with the same $Fo \times Ste$ in the phase change process, which suggests that the average temperature of the heating wall for Case 6 is relatively lower, and increasing the number of fins is good for controlling the temperature of the heating wall. However, it is found that at inclination angles of 0°, 30°, 60°, and 90°, the $\overline{Nu}$ for metal foam-fin hybrid structures with the increasing number of fins presents a slight difference. Combined with the previous analysis, the insertion of more fins causes the existence of temperature differences among different partitioned areas. It is known from the variation of $\overline{Nu}$ that even if the inclination angle increases, this temperature difference does not cause a large amount of heat to accumulate in the top area, increasing the average temperature of the heating wall. Therefore, the insertion of more fins provides better performance in terms of average temperature control on the heating wall.

Table 3
Values of $Fo \times Ste$ for three cases at four inclination angles.

Case	$Fo \times Ste$			
	0°	30°	60°	90°
4	0.461	0.506	0.509	0.524
5	0.446	0.468	0.475	0.482
6	0.415	0.432	0.438	0.443

In this study, the optimized heat transfer performance of the metal foam-fin hybrid structure has been confirmed for the goal of reducing the melting time, and the increasing number of fins can further enhance the melting rate and reduce the average temperature of the heating wall. However, it is undeniable that the addition of metal foam and fins occupy the space of PCM. Therefore, selecting the appropriate metal foam-fin hybrid structures and evaluating their heat transfer performance and energy storage efficiency is crucial for the LHTES systems. To show the influence of metal foam-fin hybrid structure on energy storage performance, energy storage density per unit volume (Q_V) for six cases is determined by the following Eq. (19):

$$Q_V = \frac{\int_0^{V_{PCM}} \rho \left[C_p(T - T_m) + f \cdot La\right] dV}{V_{container}} \tag{19}$$

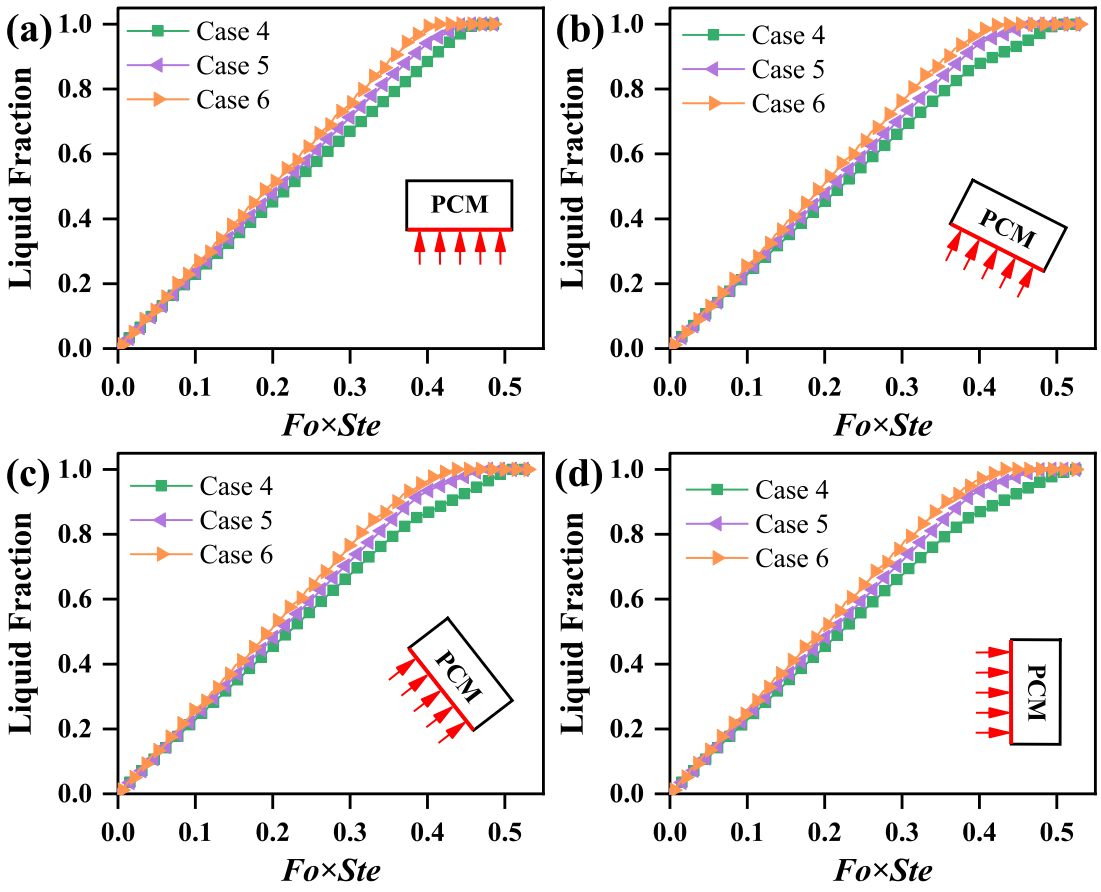

Fig. 12. Comparison of liquid fraction for Cases 4, 5, and 6 at inclination angles of (a) 0°, (b) 30°, (c) 60°, and (d) 90°.

where under the assumption of a unit width container enclosure, V_{PCM} and $V_{container}$ are the volumes of PCM and container. T is the average temperature of the container at the liquid fraction of 1.0. The Q_V for six cases at four inclination angles are compared in Fig. 14.

It shows that the Q_V monotonically decreases as a function of inclination angles within a case, and with the increase of the number of fins, the Q_V of the container enclosure with the metal foam-fin hybrid structure also decreases. There are two reasons, one is significant differences in the improvement of non-uniformity temperature due to structural variability of different cases. In the container enclosure without the metal foam-fin hybrid structure, a large amount of heat accumulates in the top area, which results in a relatively high average temperature. This phenomenon intensifies as the inclination angle increases. However, in the container enclosure with the metal foam-fin hybrid structure, a relatively low average temperature in the partitioned area leads to a decrease in energy density per unit volume. The other one is the space of PCM reduces with the increase of the number of fins. This results in less heat being stored in the PCM per unit volume of the container enclosure, which affects the energy storage density of the LHTES systems. As noticed, the quick temperature responses in the container enclosure with the metal foam-fin hybrid structure can lead to a lower average temperature and a shorter melting time, but the cost of this improvement is that the metal foam-fin hybrid structure also stores a part of thermal energy to be converted into sensible heat in the LHTES systems.

Actually, the relationship between melting rate and energy storage density per unit volume should be considered comprehensively for the design of LHTES systems. Increasing the melting rate has shown good performance through the strategy of using the metal foam-fin hybrid structure, which is conducive to the rapid storage of thermal energy. On the contrary, the simultaneous addition of the metal foam-fin hybrid structure has an adverse effect on the energy storage density per unit volume of the LHTES systems.

3.3. Prediction by artificial neural network

Based on the above discussion about the effects of melting time, inclination angles, and number of fins on the heat transfer performance of the LHTES systems, an MLPNN considering $Fo \times Ste$, θ, and n as inputs and the f and $\overline{Nu}$ as targets is designed. The optimum number of hidden neurons is firstly determined for a single hidden layer MLPNN, which is determined using the trial-and-error procedure. Fig. 15(a) shows the values of MSE for overall datasets as a function of hidden neurons number for the prediction of the f and $\overline{Nu}$. It can be found that the values of MSE for overall datasets of the f and $\overline{Nu}$ decrease by increasing the number of hidden neurons up to ten and twelve, respectively, and thereafter little improvement is seen. Therefore, MLPNN with ten and twelve hidden neurons is the optimum structure for accurate prediction of the f and $\overline{Nu}$. Fig. 15(b) shows the change of statistical indicator MSE for the MLP-GA model with ten and twelve hidden neurons varying the generation parameter. The results suggest that the process of improvement and elitism occurs with the evolution of generations. The amount of errors decreases, and an improved result is chosen after multiple repetitions. Besides, the generation parameter of 100 is appropriate to the prediction of the targets, which is attributed to a limited change in the amount of errors after generation repetition.

Generally, having a training and test data set is the basis of supervised machine learning, which has an important influence

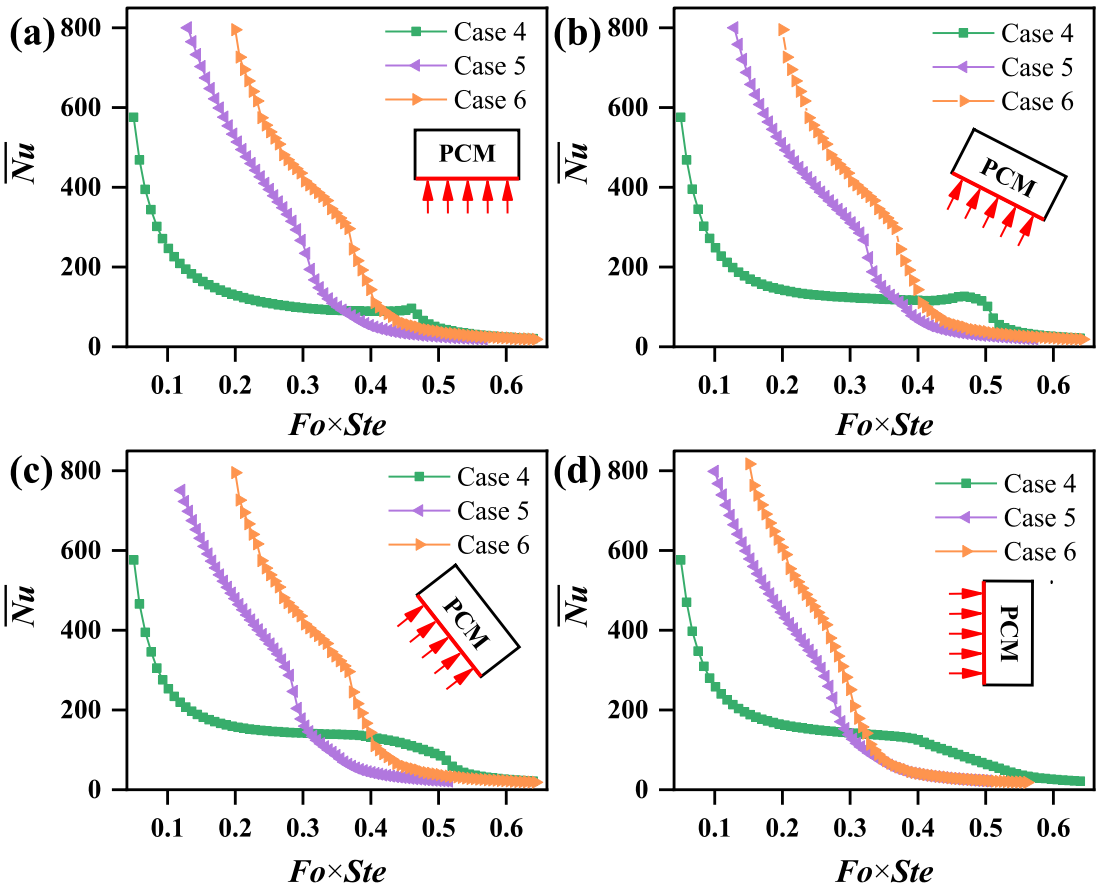

Fig. 13. Comparison of average Nusselt number for Cases 4, 5, and 6 at inclination angles of (a) 0°, (b) 30°, (c) 60°, and (d) 90°.

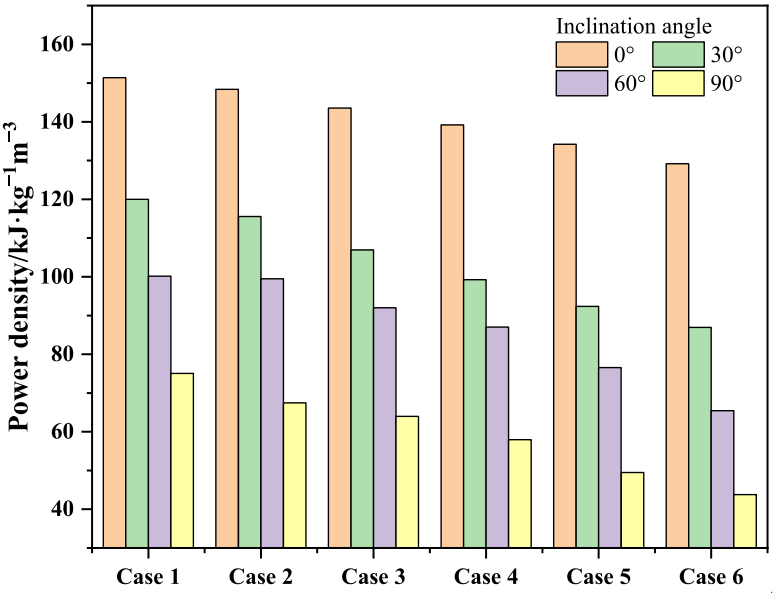

Fig. 14. Energy storage density per unit volume at the liquid fraction of 1.0.

on the accuracy of models. In this study, the accurate operation of the presented model is assured by the MLP-GA model. The performance of the proposed approach is evaluated by plotting the actual numerical values against their predicted values by the constructed model for both training and testing datasets.

Figs. 16 and 17 illustrate the efficiencies and remarkable capabilities of the proposed MLP-GA model for predicting the f and $\overline{Nu}$, including the training, testing, and overall datasets. A solid black line with the inclination angle of 45° indicates the perfect fit, meaning that the predicted values equal to the actual

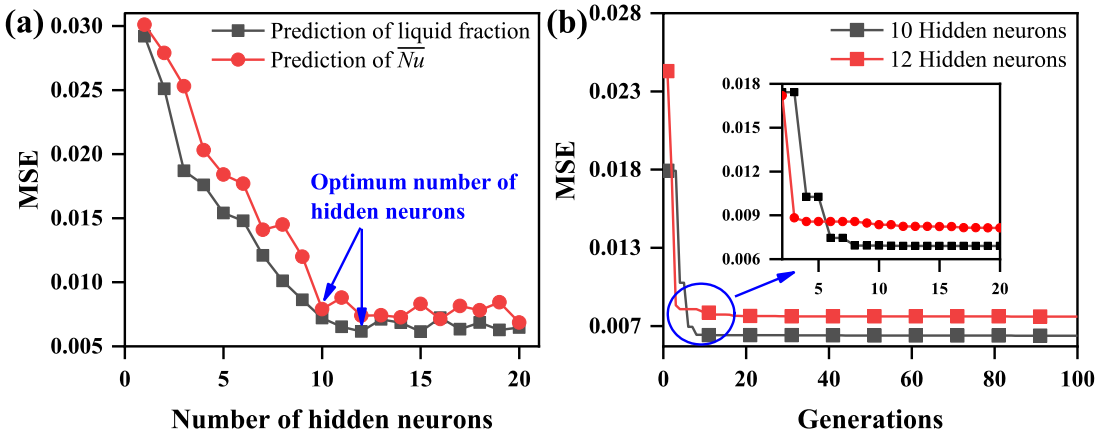

Fig. 15. (a) MSE for various MLPNN for overall subsets of the liquid fraction and average Nusselt number, and (b) Statistical indicator MSE for MLP-GA model with ten and twelve hidden neurons varying the generation parameter.

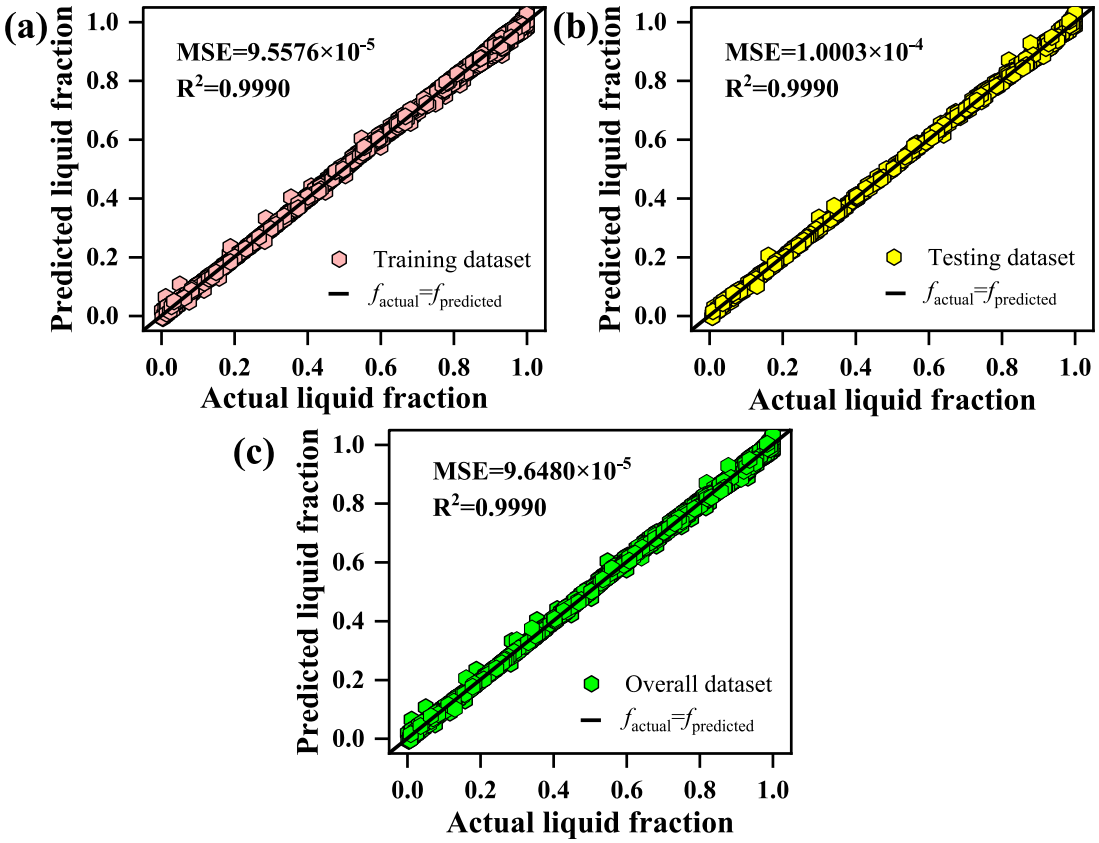

Fig. 16. Parity plot of liquid fraction predicted by MLP-GA model versus actual numerical values of (a) training, (b) testing, and (c) overall datasets.

numerical values. The statistics for prediction performance of the f and $\overline{Nu}$ on the training, testing, as well as overall datasets, are presented in Table 4. For the prediction of the f, the evaluation indicators of MSE and R^2 are 9.6480 × 10^{-5} and 0.9990 between the predicted values and the actual values in the overall datasets. For the prediction of the $\overline{Nu}$, the evaluation indicators of MSE and R^2 are 0.0150 and 0.9937 between the predicted values and the actual values in the overall datasets. The results indicate those good agreements of the f and $\overline{Nu}$ exist between the data obtained from the predications of the MLP-GA model and the actual numerical data. According to the predicted data associated with each process of the MLP-GA model, this model exhibits a great sensitivity probably to melting time and the number of fins and a conspicuous correlation of inclination angles.

Table 4
Statistics for prediction performance of the f and $\overline{Nu}$ on the training, testing as well as overall datasets.

Optimal target	Process	MSE	R^2
f	Training	9.5576 × 10^{-5}	0.9990
	Testing	1.0003 × 10^{-4}	0.9990
	Overall	9.6480 × 10^{-5}	0.9990
$\overline{Nu}$	Training	0.0148	0.9938
	Testing	0.0156	0.9935
	Overall	0.0150	0.9937

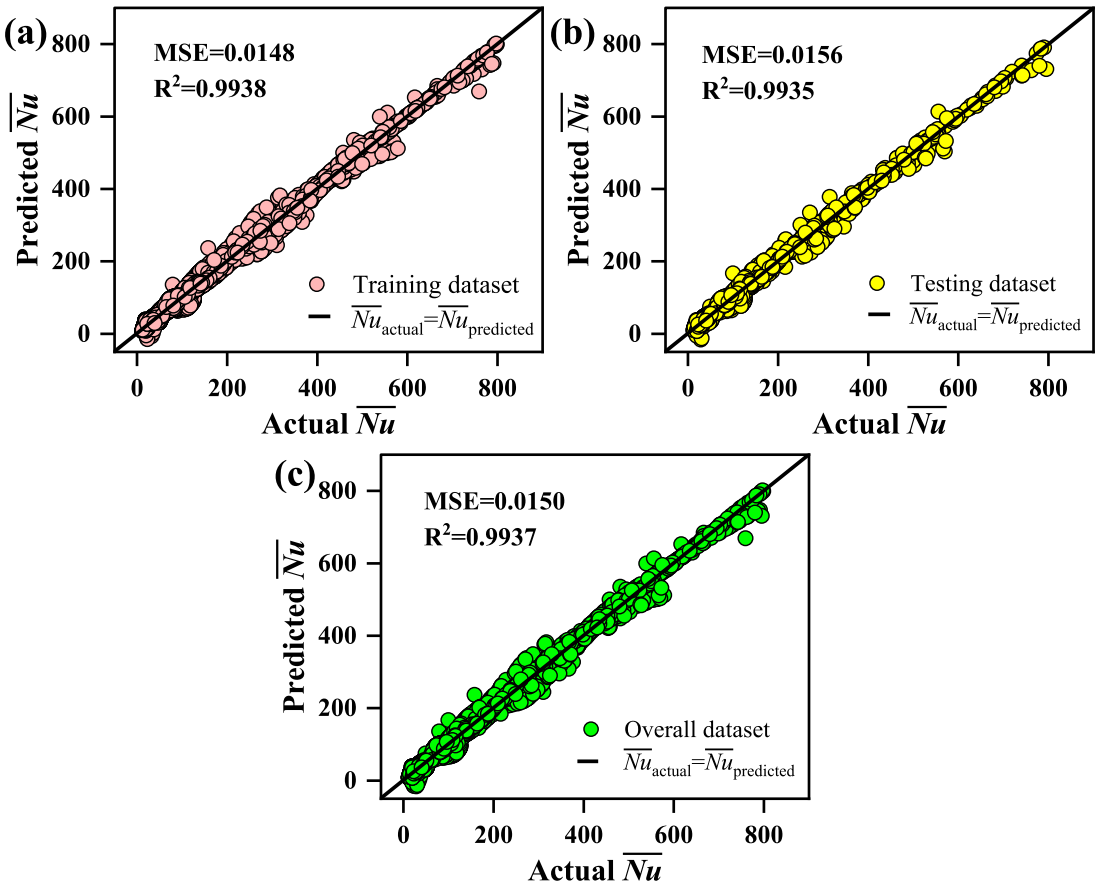

Fig. 17. Parity plot of average Nusselt number predicted by MLP-GA model versus actual numerical values of (a) training, (b) testing, and (c) overall datasets.

4. Conclusions

Due to the low thermal conductivity of PCM, the hybrid metal foam-fin structure can be employed to improve the heat transfer performance of PCM in the LHTES systems. This study numerically investigates the effects of the hybrid metal foam-fin structure on the heat transfer performance of PCM at different inclination angles. The inclination angles of container enclosure are set at 0°, 30°, 60°, and 90°, and the heat transfer performances of PCM enhanced by fin, metal foam, and metal foam-fin hybrid structures are compared, including the solid–liquid phase interfaces, streamlines, liquid fraction (f), the dimensionless time ($Fo \times Ste$), and average Nusselt number ($\overline{Nu}$) of PCM. Besides, the f and $\overline{Nu}$ during the phase change process are predicted by the ANN. The main conclusions can be drawn as follows:

(1) The metal foam-fin hybrid structure can improve the heat transfer performance of PCM, attributed to the heat transferred from the heating wall to the interior of the LHTES systems by fins and further distributed deeply into PCM by metal foam. Compared to the $Fo \times Ste$ of pure PCM, that of metal foam-1 fin hybrid structure is reduced by 52.69% at the inclination angle of 90°, and the higher $\overline{Nu}$ can be obtained at four inclination angles.

(2) As the inclination angle increases, inserting more fins into PCM can improve the heat transfer performance and reduce heat accumulation in the top area, due to the insertion of more fins working in synergy with foam metal to provide better temperature control performance in the LHTES systems. Compared to the $Fo \times Ste$ of pure PCM, that of metal foam-5 fins hybrid structure is reduced by 60.02% at the inclination angle of 90°.

(3) A comprehensive consideration of the relationship between melting rate and energy storage density per unit volume is necessary for the design of LHTES systems. Increasing the melting rate has shown the ideal performance through the strategy of using the metal foam-fin hybrid structure, which is conducive to the rapid storage of thermal energy. On the contrary, the simultaneous addition of the metal foam-fin hybrid structure has an adverse effect on the energy storage density per unit volume of the LHTES systems.

(4) The MLP-GA model shows good predictions of f and $\overline{Nu}$ during the phase change process with MSE and R^2 of 9.6480×10^{-5}, 0.9990 and 0.0150, 0.9937, respectively. The prediction results are highly sensitive to the melting time and the number of fins and a conspicuous correlation of inclination angles.

CRediT authorship contribution statement

Wei Cui: Writing – original draft, Conceptualization, Methodology, Data curation. **Tianyu Si:** Writing – review & editing, Methodology. **Xiangxuan Li:** Investigation, Writing – review & editing. **Xinyi Li:** Methodology, Writing – review & editing. **Lin Lu:** Writing – review & editing. **Ting Ma:** Writing – review & editing. **Qiuwang Wang:** Writing – review & editing, Supervision, Funding acquisition.

Declaration of competing interest

The authors declare that they have no known competing financial interests or personal relationships that could have appeared to influence the work reported in this paper.

Acknowledgments

This work was supported by the National Natural Science and Hong Kong Research Grant Council Joint Research Funding Project of China (Grant No. 51861165105), the Foundation for Innovative Research Groups of the National Natural Science Foundation of China (Grant No. 51721004), and the Research Grants Council of Hong Kong, China and the National Natural Science Foundation of China (Project No. N_PolyU513/18).

References

Ling, Z., Zhang, Z., Shi, G., Fang, X., Wang, L., Gao, X., et al., 2014. Review on thermal management systems using phase change materials for electronic components, li-ion batteries and photovoltaic modules. Renew. Sustain. Energy Rev. 31, 427–438.

Tyagi, V.V., Chopra, K., Kalidasan, B., Chauhan, A., Stritih, U., An, S., et al., 2021. Phase change material based advance solar thermal energy storage systems for building heating and cooling applications: A prospective research approach. Sustain. Energy Technol. Assess. 47.

Luo, J., Zou, D., Wang, Y., Wang, S., Huang, L., 2022. Battery thermal management systems (BTMs) based on phase change material (PCM): A comprehensive review. Chem. Eng. J. 430.

Li, D., Wang, J., Ding, Y., Yao, H., Huang, Y., 2019. Dynamic thermal management for industrial waste heat recovery based on phase change material thermal storage. Appl. Energy 236, 1168–1182.

Alva, G., Liu, L., Huang, X., Fang, G., 2017. Thermal energy storage materials and systems for solar energy applications. Renew. Sustain. Energy Rev. 68, 693–706.

Zhang, N., Yuan, Y., Cao, X., Du, Y., Zhang, Z., Gui, Y., 2018. Latent heat thermal energy storage systems with solid–liquid phase change materials: A review. Adv. Eng. Mater. 20, 1700753.

Ji, C., Qin, Z., Low, Z., Dubey, S., Choo, F.H., Duan, F., 2018. Non-uniform heat transfer suppression to enhance PCM melting by angled fins. Appl. Therm. Eng. 129, 269–279.

Sodhi, G.S., Muthukumar, P., 2021. Compound charging and discharging enhancement in multi-PCM system using non-uniform fin distribution. Renew. Energy 171, 299–314.

Oya, T., Nomura, T., Okinaka, N., Akiyama, T., 2012. Phase change composite based on porous nickel and erythritol. Appl. Therm. Eng. 40, 373–377.

Sami, S., Etesami, N., 2017. Improving thermal characteristics and stability of phase change material containing TiO_2 nanoparticles after thermal cycles for energy storage. Appl. Therm. Eng. 124, 346–352.

Ali, H.M., Arshad, A., 2017. Experimental investigation of n-eicosane based circular pin-fin heat sinks for passive cooling of electronic devices. Int. J. Heat Mass Transfer 112, 649–661.

Hosseinizadeh, S.F., Tan, F.L., Moosania, S.M., 2011. Experimental and numerical studies on performance of PCM-based heat sink with different configurations of internal fins. Appl. Therm. Eng. 31, 3827–3838.

Xiao, X., Zhang, P., Li, M., 2013. Preparation and thermal characterization of paraffin/metal foam composite phase change material. Appl. Energy 112, 1357–1366.

Liu, Z., Yao, Y., Wu, H., 2013. Numerical modeling for solid–liquid phase change phenomena in porous media: Shell-and-tube type latent heat thermal energy storage. Appl. Energy 112, 1222–1232.

Shatikian, V., Ziskind, G., Letan, R., 2005. Numerical investigation of a PCM-based heat sink with internal fins. Int. J. Heat Mass Transfer 48, 3689–3706.

Guo, J., Liu, Z., Du, Z., Yu, J., Yang, X., Yan, J., 2021. Effect of fin-metal foam structure on thermal energy storage: An experimental study. Renew. Energy 172, 57–70.

Yang, X., Yu, J., Xiao, T., Hu, Z., He, Y.-L., 2020. Design and operating evaluation of a finned shell-and-tube thermal energy storage unit filled with metal foam. Appl. Energy 261.

Zhao, C., Opolot, M., Liu, M., Bruno, F., Mancin, S., Hooman, K., 2020. Numerical study of melting performance enhancement for PCM in an annular enclosure with internal-external fins and metal foams. Int. J. Heat Mass Transfer 150.

Yang, C., Xu, Y., Cai, X., Zheng, Z.-J., 2021a. Melting behavior of the latent heat thermal energy storage unit with fins and graded metal foam. Appl. Therm. Eng. 198, 117462.

Ding, C., Wang, L., Niu, Z., 2021. Thermal performance evaluation of latent heat storage systems with plate fin-metal foam hybrid structure. Case Stud. Therm. Eng. 27, 101309.

Yang, X., Niu, Z., Guo, J., Bai, Q., Li, H., He, Y.-L., 2020. Role of pin fin-metal foam composite structure in improving solidification: Performance evaluation. Int. Commun. Heat Mass Transfer 117.

Yang, X., Xu, F., Wang, X., Guo, J., Li, M.-J., 2021b. Solidification in a shell-and-tube thermal energy storage unit filled with longitude fins and metal foam: A numerical study. Energy Built. Environ..

Be´nard, C., Gobin, D., Martinez, F., 1985. Melting in rectangular enclosures: Experiments and numerical simulations. J. Heat Transfer 107, 794–803.

Ho, C., Viskanta, R., 1984. JJo HT-toTA. Heat transfer during melting from an isothermal vertical wall. 106 pp. 12-19.

Omari, K.E., Kousksou, T., Guer, Y.L., 2011. Impact of shape of container on natural convection and melting inside enclosures used for passive cooling of electronic devices. Appl. Therm. Eng. 31, 3022–3035.

Ozoe, H., Sayama, H., Churchill, S.W., 1975. Natural convection in an inclined rectangular channel at various aspect ratios and angles—experimental measurements. Int. J. Heat Mass Transfer 18, 1425–1431.

Kamkari, B., Shokouhm, H., Bruno, F., 2014. Experimental investigation of the effect of inclination angle on convection-driven melting of phase change material in a rectangular enclosure. Int. J. Heat Mass Transfer 72, 186–200.

Yang, X., Guo, Z., Liu, Y., Jin, L., He, Y.-L., 2019. Effect of inclination on the thermal response of composite phase change materials for thermal energy storage. Appl. Energy 238, 22–33.

Kothari, R., Sahu, S.K., Kundalwal, S.I., Sahoo, S.P., 2021. Experimental investigation of the effect of inclination angle on the performance of phase change material based finned heat sink. J. Energy Storage 37.

Sathe, T., Dhoble, A.S., 2019. Thermal analysis of an inclined heat sink with finned PCM container for solar applications. Int. J. Heat Mass Transfer 144.

Zheng, H., Wang, C., Liu, Q., Tian, Z., Fan, X., 2018. Thermal performance of copper foam/paraffin composite phase change material. Energy Convers. Manage. 157, 372–381.

Xu, Y., Zheng, Z.-J., Yang, C., Cai, X., 2021. Intelligent optimization of horizontal fins to improve the melting performance of phase change materials in a square cavity with isothermal vertical wall. J. Energy Storage 44.

Motahar, S., Jahangiri, M., 2020. Transient heat transfer analysis of a phase change material heat sink using experimental data and artifificial neural network. Appl. Therm. Eng. 114817.

Cui, W., Li, X., Li, X., Lu, L., Ma, T., Wang, Q., 2022. Combined effects of nanoparticles and ultrasonic field on thermal energy storage performance of phase change materials with metal foam. Appl. Energy 309, 118465.

Voller, V.R., Prakash, C., 1987. A fixed grid numerical modelling methodology for convection–diffusion mushy region phase-change problems. Int. J. Heat Mass Transfer 30, 1709–1719.

Tian, Y., Zhao, C.Y., 2011. A numerical investigation of heat transfer in phase change materials (PCMs) embedded in porous metals. Energy 36, 5539–5546.

Fourie, G., Du Plessis, P., 2002. Pressure drop modelling in cellular metallic foams. Chem. Eng. Sci..

Parsazadeh, M., Malik, M., Duan, X., McDonald, A., 2021. Numerical study on melting of phase change material in an enclosure subject to Neumann boundary condition in the presence of Rayleigh-Bénard convection. Int. J. Heat Mass Transfer 171, 121103.